Macromolecules
ARTICLE

Macromolecules **2010**, *43*, 5295–5305 **5295**
DOI: 10.1021/ma100347k

Synthesis and Characterization of Elastomeric Heptablock Terpolymers Structured by Crystallization

C. Guillermo Alfonzo,[†] Guillaume Fleury,[†,§] Kimberly A. Chaffin,[‡] and Frank S. Bates*[,†]

[†]*Department of Chemical Engineering and Materials Science, University of Minnesota, Minneapolis, Minnesota 55455, and* [‡]*Corporate Science and Technology, Medtronic, Inc., Minneapolis, Minnesota 55432.* [§]*Current address: Laboratoire de Chimie des Polymères Organiques, Université Bordeaux 1/CNRS, Ecole Nationale Supérieure de Chimie, de Biologie & de Physique, 16 Avenue Pey-Berland, 33607 Pessac Cedex, France*

Received February 11, 2010; Revised Manuscript Received May 8, 2010

ABSTRACT: We report the synthesis and characterization of fully saturated hydrocarbon block copolymer thermoplastic elastomers with competitive mechanical properties and attractive processing features. Block copolymers containing glassy poly(cyclohexylethylene) (C), elastomeric poly(ethylene-*alt*-propylene) (P), and semicrystalline poly(ethylene) (E) were produced in a CEC−P−CEC heptablock architecture, denoted XPX, by anionic polymerization and catalytic hydrogenation. The X blocks contain equal volume fractions of C and E, totaling 40%−60% of the material overall. All the XPX polymers are disordered above the melt temperature for E ($T_{m,E} \cong 95$ °C) as evidenced by SAXS and dynamic mechanical spectroscopy measurements. Cooling below $T_{m,E}$ results in crystallization of the E blocks, which induces microphase segregation of E, C, and P into a complex morphology with a continuous rubbery domain and randomly arranged hard domains as shown by TEM. This mechanism of segregation decouples the processing temperature from the XPX molecular weight up to a limiting value. Tensile mechanical testing (simple extension and cyclic loading) demonstrates that the tensile strength (ca. 30 MPa) and strain at break (> 500%) are comparable to the behavior of CPC triblock thermoplastic elastomers of similar molecular weight and glass content. However, in the CPC materials, processability is constrained by the order−disorder transition temperature, limiting the applications of these materials. Elastic recovery of the XPX materials following seven cycles of tensile deformation is correlated with the fraction of X in the heptablock copolymer, and the residual strain approaches that of CPC when the fraction of hard blocks $f_X \leq 0.39$.

Introduction

Block copolymers (BCPs) containing a matrix of rubbery blocks, anchored on both ends to thermodynamically incompatible and hard (glassy or semicrystalline) blocks, are generally referred to as thermoplastic elastomers (TPEs).[1,2] Poly(styrene-*b*-isoprene-*b*-styrene) (SIS) triblock copolymers are the most familiar commercial products that fall into this category. Two temperatures control the properties and processing of these materials. Above the hard block glass transition temperature ($T_{g,S} \cong$ 100 °C) the material softens and can be deformed irreversibly; in this temperature range the rheological properties are dominated by the microphase structure. Further heating the material can lead to a state of disorder and liquid-like rheological properties. However, the point at which this transition occurs, known as the order−disorder transition temperature (T_{ODT}), is directly dependent on the overall molecular weight for a given composition; increasing the molecular weight increases T_{ODT}.[3] Many applications of TPEs require balancing molecular weight against processing requirements that favor a low T_{ODT} (i.e., low processing temperature) in order to minimize polymer degradation and equipment needs. Choosing different block types (e.g., hydrogenated poly(butadiene) instead of poly(isoprene)) necessitates a reevaluation of the relationships between room temperature properties and processing, each dependent on the molecular weight. This publication describes a new approach to designing thermoplastic elastomers that decouples T_{ODT} from the overall block copolymer molecular weight.

Microphase separation of thermodynamically compatible block copolymers also can be induced by crystallization.[4−11] In this situation the transition from a state of microphase separation to spatial homogeneity is determined by the crystal melting temperature (T_m) and does not depend on the block copolymer molecular weight. Several groups have demonstrated this effect, including Hotta et al.,[10] who reported on poly(propylene)-based BPCs containing amorphous and rubbery midblocks and semicrystalline end-blocks, and Koo et al., who developed EPE triblock[8] and $(EP)_n$ multiblock copolymers,[9] where E is semicrystalline poly(ethylene) and P is rubbery poly(ethylene-*alt*-propylene). The $(EP)_n$ materials, which are produced by hydrogenating anionically polymerized poly(1,4-butadiene-*b*-1,4-isoprene)$_n$ multiblock copolymers, are characterized by a small Flory−Huggins χ parameter. Below a threshold block molecular weight ($M = M_E = M_P < 50\,000$ g/mol) these materials are disordered above $T_{m,E}$. Microphase separation is induced by crystallization upon cooling the homogeneous melt. Because of a finite, albeit small, segment−segment interaction parameter, increasing M above the critical value leads to ordering in the melt state. Koo et al. demonstrated two limiting types of mechanical properties in these block copolymers at room temperature. Crystallization-induced segregation results in a relatively weak material with a tensile strength of $\sigma_{TS} \leq 10$ MPa (also reported in the poly(propylene) system by Hotta et al.) while cooling and crystallizing higher molecular weight ($n > 8$) $(EP)_n$

*To whom correspondence should be addressed. E-mail: bates@cems.umn.edu.

Published on Web 05/19/2010

polymers led to $\sigma_{TS} \approx 20-30$ MPa. The authors reasoned that these results could be traced to the orientation and inherent strength of the E crystals within the melt ordered morphologies and the reinforcing effect created by a large number of blocks even in the case of melt disorder. Thus, for crystalline and rubber block copolymers, crystallization-induced segregation tends to produce mechanically weak materials unless they are constructed with many blocks, which is often impractical. Also, regardless of the segregation mechanism, high strength values are only achieved with high volume fractions of E (> 50%), which compromises the low strain elastic response and results in significant irreversible plastic deformation.[11−14]

Another recently reported strategy for tailoring the mechanical properties of polyolefin block copolymers is to combine three basic physical states—rubbery, glassy, and semicrystalline—in a multiblock copolymer architecture. Mahanthappa et al.[14,15] produced CPEPC pentablock copolymers containing 40 vol % glassy C, or poly(cyclohexylethylene), derived from hydrogenating polystyrene, and varying proportions of semicrystalline E and rubbery P. Despite relatively low overall molecular weights (30−40 kg/mol) these saturated terpolymers microphase separate into a lamellar structure at elevated temperatures, which is preserved upon cooling below $T_{g,C} \cong 135$ °C, and subsequent crystallization of the E domains below 90 °C. These composite materials exhibit tensile strengths between 25 and 38 MPa accompanied by an elastic modulus intermediate to a rubber and plastic ($E \sim 50-100$ MPa). Balsamo et al.[16,17] and Schamlz et al.[13,18] have combined similar types of monomers in producing ABC systems, where A is glassy, B is rubbery, and C is semicrystalline. These all have relatively high molecular weights (80−219 kg/mol) and are strongly segregated due to the chemical incompatibility between blocks. Although these polymers contain semicrystalline blocks, the ultimate processing conditions are governed by T_{ODT}, which is coupled to the overall molecular weight.

Fleury and Bates[19] recently showed that an undecablock copolymer of the type CECEC−P−CECEC containing 50% P, 25% E, and 25% C and a modest overall molecular weight of 87 000 g/mol was disordered above the melting temperature of the E blocks. Yet this material displayed excellent elastic properties at room temperature (e.g., $\sigma_{TS} = 32$ MPa and a strain at break $\varepsilon_b >$ 1500%). This finding suggests that the synergistic combination of crystallization-induced segregation accompanied by partial vitrification offers an attractive method of producing competitive thermoplastic elastomers that can be processed as relatively inviscid, homogeneous liquids at a temperature determined by the melting point of the semicrystalline blocks, i.e., independent of the overall molecular weight up to a limiting value.

This article expands on this idea, through an in-depth study of a basic hierarchical block copolymer architecture suitable for creating crystallization-induced thermoplastic elastomers: CEC−P−CEC heptablock copolymers. Here we demonstrate that at modest molecular weights these multiblocks are homogeneous (disordered) above about 100 °C, i.e., T_m of E, due to a favorable balance between the three χ_{ij} parameters that define the mixing thermodynamics. Cooling below $T_{m,E}$ results in partial crystallization of E, which induces segregation and vitrification of C, leading to a class of microphase-separated materials that have a common processing temperature, independent of molecular weight for $M \leq 114\,000$ g/mol. This combination of glassy (C) and semicrystalline (E) hard blocks results in thermoplastic elastomers with competitive strengths and in certain limits excellent elastic recovery. Five CEC−P−CEC heptablock terpolymers were synthesized, each with equal volume fractions of C and E and between 40 and 60 vol % P. We have characterized the phase behavior of these specimens by differential scanning calorimetry (DSC) and dynamic mechanical spectroscopy (DMS), small-angle X-ray scattering (SAXS), and transmission electron microscopy (TEM). The mechanical properties were measured in tension by simple extension and cyclic loading, and these results are compared with conventional CPC triblock copolymer elastomers prepared with similar C contents.

Experimental Section

Block Copolymer Synthesis and Hydrogenation. Triblock copolymer CPC-1 was obtained from The Dow Chemical Co., while CPC-2 and the CEC−P−CEC heptablock copolymers were produced at the University of Minnesota. A SIS precursor triblock was synthesized by sequential living anionic polymerization of styrene (S) (Aldrich), isoprene (I) (Acros Organics), and S in purified cyclohexane (Fischer Scientific) at 40 °C, initiated with *sec*-butyllithium (1.4 M solution in cyclohexane, Aldrich), as described elsewhere.[20] For the heptablock copolymers, living SBS-I^-,Li^+ copolymers were prepared by sequential polymerization of S, butadiene (B) (Aldrich), S, and I as noted above and subsequently coupled using a stoichiometric amount of α,α′-dibromo-*p*-xylene (Aldrich) added in a dropwise fashion until solution became colorless (about 4−6 h) to produce the precursor SBS−I−SBS materials. In all cases the overall fraction of S and B added to the reactor was held constant. An aliquot of the completed first S block was drawn after 8 h of reaction time and precipitated in degassed methanol (Aldrich) for further analysis. SIS and SBS−I−SBS were hydrogenated to yield CPC and CEC−P−CEC, respectively. This was accomplished by reaction for 12 h over a Pt/Re catalyst supported on macroporous silica particles (Dow Chemical) in degassed cyclohexane at 170 °C under 500 psig of H_2.[21] Block copolymers were recovered from solution in all cases by precipitation in a 1:3 (volume ratio) mixture of isopropanol and methanol followed by drying at room temperature under vacuum to constant weight. We will refer to CEC−P−CEC as XPX based on the pseudo-triblock geometry.

Molecular Characterization. Block copolymer compositions were determined from quantitative ^{1}H nuclear magnetic resonance (NMR) spectra collected on the unsaturated polymers in deuterated chloroform ($CDCl_3$) (99.8%, Aldrich) using a Varian Unity Inova 300 spectrometer. Monomer mole fractions were calculated by integrating resonances associated with S, B, and I repeat units; these values were then converted to volume fractions for the saturated compounds using the following published polymer densities at 140 °C:[22] $\rho_C = 0.920$ g/cm^3; $\rho_E = 0.784$ g/cm^3; $\rho_P = 0.790$ g/cm^3. These spectra also confirmed that the isoprene and butadiene polymerizations resulted in predominantly 1,4-monomer addition, with 6−8 mol % 4,3-I and 10−12 mol % 1,2-B, respectively. ^{1}H NMR spectra were also recorded from the hydrogenated polymers in deuterated chloroform at room temperature for CPC and in deuterated toluene (C_7D_8) (99.6%, Aldrich) at 70 °C for XPX to establish the extent of saturation for each polymer, which in every case was greater than 97%. The number-average molecular weight, $M_{n,S}$, of the first S block of each block copolymer and the molecular weight distribution (M_w/M_n), or polydispersity, of all polymers were determined by size exclusion chromatography (SEC). A Waters 717 GPC fitted with three Polymer Laboratories Mixed-C columns and operated at 30 °C with tetrahydrofuran (J.T. Baker) and calibrated with polystyrene standards was employed with the unsaturated polymers and with CPC. The saturated XPX polymers were characterized with a PL-GPC 220 system operated at 135 °C with 1,2,4-trichlorobenzene. Monomodal and relatively narrow distribution ($M_w/M_n < 1.21$) peaks were recorded in all cases. Saturated polymer molecular weights were calculated based on $M_{n,S}$ and the overall composition derived from the reaction stoichiometry and NMR results.

Differential Scanning Calorimetry (DSC). Thermal transitions (glass transition and melting and crystallization temperatures) were determined using a TA Instruments Q1000

Scheme 1. Molecular Structure of CEC−P−CEC Heptablock Copolymers

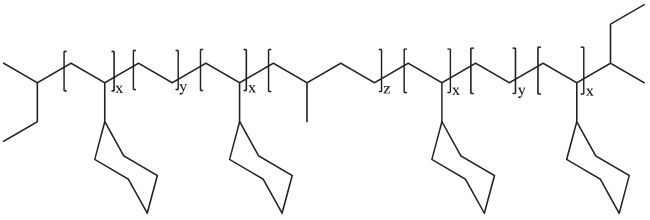

differential scanning calorimeter (DSC). Poly(ethylene) fractional crystallinity, X_c, was calculated using the expression $X_c = (\Delta H_m/w_E)\rho H°_{m,E}$ where w_E is the weight fraction of E and $\Delta H_m = 277$ J g^{-1} is the theoretical heat of melting for the 100% crystalline poly(ethylene).[23] Samples were heated to 160 °C, cooled to −80 °C, and heated back to 160 °C, all at 10 °C/min.

Dynamic Mechanical Spectroscopy (DMS). A Rheometrics Scientific ARES rheometer equipped with 25 or 8 mm diameter parallel plates was used to determine the elastic, G', and viscous, G'', dynamic moduli over the frequency range $0.01 \leq \omega \leq 100$ rad/s. All measurements were conducted at a strain of 1%, within the linear viscoelastic regime. Two types of tests were used to probe the order−disorder, melting, and crystallization transitions: isothermal frequency sweeps and isochronal temperature sweeps at fixed heating or cooling rates of between 0.5 and 2 °C/min.[3,24]

Small-Angle X-ray Scattering (SAXS). Synchrotron-source SAXS was performed on the saturated block copolymers at Argonne National Laboratory (Argonne, IL) using the DuPont−Northwestern−Dow Collaborative Access Team (DND-CAT) facility with a beam wavelength of $\lambda = 0.729$ Å and a sample-to-detector distance of 6.53 m. Calibration was achieved with silver behenate, and data were collected on a Mar CCD area detector. Experiments were performed on unaligned powder like XPX specimens that were molded at 170 °C and then cooled to room temperature. XPX samples were heated to about 180 °C for 3 min to erase thermal history and then cooled at about 30 °C/min and held for 3 min at either 140 or 25 °C, where 2-D patterns were collected. Laboratory source SAXS was performed at the Institute of Technology Characterization Facility at the University of Minnesota using Cu Kα X-rays from a Rigaku RU-200VBH rotating anode and a sample-to-detector distance of 4.41 m. CPC samples were shear aligned prior to the experiment to improve the state of long-range order, and synchrotron SAXS data were collected at 25 °C for CPC-1 and laboratory SAXS data were collected at 150 °C for CPC-2 without any additional thermal treatment. Alignment of the cylindrical structures in the CPC copolymers was achieved using the large-amplitude reciprocating shear device described by Koppi.[25] Compression-molded samples 20 mm long by 10 mm wide by 1 mm thick were sheared under argon for about 2 h at $T_{ODT} - 10$ °C with a strain amplitude of 200% and a shear rate of 0.5 s^{-1}. Two-dimensional scattering data were azimuthally integrated to obtain plots of intensity I vs scattering wavevector modulus q ($q = (4\pi/\lambda)\sin(\theta/2)$, where θ is the scattering angle).

Transmission Electron Microscopy (TEM). TEM experiments were performed at the Institute of Technology Characterization Facility at the University of Minnesota with a JEOL 1210 electron microscope in the bright field mode operating at 110 kV. Samples were cryo-microtomed at −120 °C with a diamond knife to produce a flat surface and subsequently stained with ruthenium oxide (RuO_4) for 4 h using reported procedures[26] to create contrast between chemically distinct domains. Stained samples were microtomed again at −120 °C, and 70−100 nm thick specimens were collected for imaging.

Mechanical Testing. Samples were drawn in tension up to the point of failure in a Rheometrics Scientific MINIMAT uniaxial tensile testing instrument fitted with a 200 N load cell.

Table 1. Molecular Characterization Data for CPC and XPX Copolymers

sample	f_C	f_E	f_P	N^a	M_n (g/mol)	$M_w/M_n{}^b$
CPC-1	0.18	0.00	0.82	1193	90 050	1.04
CPC-2	0.30	0.00	0.70	597	47 400	1.03
XPX-1	0.18	0.22	0.60	1450	103 400	1.11
XPX-2a	0.25	0.26	0.49	808	59 000	1.11
XPX-2b	0.25	0.26	0.49	1086	79 200	1.13
XPX-2c	0.25	0.26	0.49	1560	113 700	1.16
XPX-3	0.30	0.28	0.42	592	43 800	1.21

[a] Calculated using bulk homopolymer densities from Fetters et al.[22] with 118 Å^3 reference volume. [b] Determined for saturated CPC and for unsaturated precursors of XPX by SEC with PS standards in THF at 30 °C.

All experiments were conducted at room temperature and at a constant rate of 200% strain/min. Rectangular bars 11 mm long, 2−3 mm wide, and 0.8−1.2 mm thick were employed, with a 5−7 mm gauge length (l_0) and a 2−3 mm^2 initial cross-sectional area (A_0). This geometry is the best one to avoid slipping and easily set up the sample in the instrument so that it can be stretched to high strains. Engineering stress (σ) vs nominal strain (ε) curves were obtained from force (F) vs displacement (Δl) data, where $\sigma = F/A_0$ and $\varepsilon = \Delta l/l_0$. Young's modulus E was determined by fitting the linear regime of the stress−strain curve, below about 10% strain, with $\sigma = E\varepsilon$. The data reported here represent values averaged over eight specimens tested per material. Tension set (%), ε_s, calculated as (final gauge length $- l_0)/l_0 \times 100$, was determined for each sample. Similar samples were used to run cyclic extension−compression tests at room temperature and a constant rate of 200% strain/min. A series of seven cycles, each including application of a 400% strain followed by a return back to 0% strain, constituted a complete strain recovery experiment. Residual strain, which is reported for each cycle, is defined here as the strain remaining at zero stress following a sequence of extension and compression. At least three specimens of each material were tested in this manner.

Results and Analysis

Synthesis. Three types of CEC−P−CEC copolymers, abbreviated XPX and shown in Scheme 1, were produced in this study, with C volume fractions of 18%, 25%, and 30% and similar corresponding volume fractions of E.

At a composition of 25 vol % C, three materials were synthesized with molecular weights of 59, 79, and 114 kg/mol, in order to investigate the role of this parameter on properties. Two CPC materials with C volume fractions of 18% (obtained from Dow Chemical) and 30% (synthesized in our laboratory) were prepared for comparison. Table 1 summarizes the basic molecular characteristics of the block copolymers employed in this study.

The final step in the polymerization of the SBS−I−SBS precursor copolymers was achieved by coupling "living" SBSI$^-$,Li$^+$ molecules. Figure 1 shows a size exclusion chromatograph (SEC) trace of the precursor materials associated with XPX-2b. Comparison of the uncoupled (SBSI$^-$) and coupled (SBS-I-SBS) forms reveals monomodal molecular weight distributions with average molecular weights that differ by a factor of ∼2. A relatively small amount of uncoupled polymer is present in the coupled product. In all cases, at least 93% coupling was achieved through these reactions. Heptablock polydispersity indices are somewhat higher than those obtained with the CPC triblock which we attribute to the relatively slow addition of butadiene to poly(styryllithium). The molecular weight distribution was not affected by hydrogenation of the unsaturated heptablock copolymers.

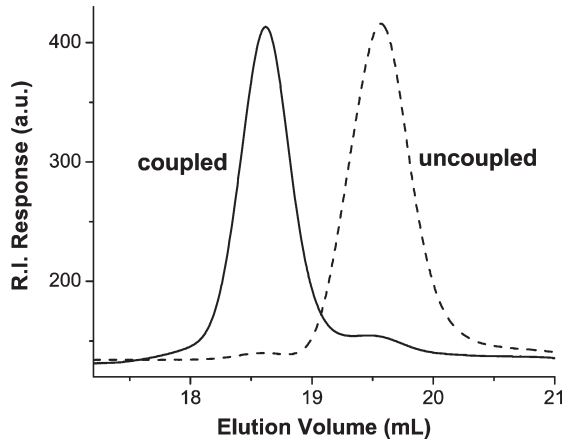

Figure 1. SEC trace for XPX-2b's precursor systems, in their uncoupled (SBSI) and coupled (SBS−I−SBS) forms, showing high coupling efficiency.

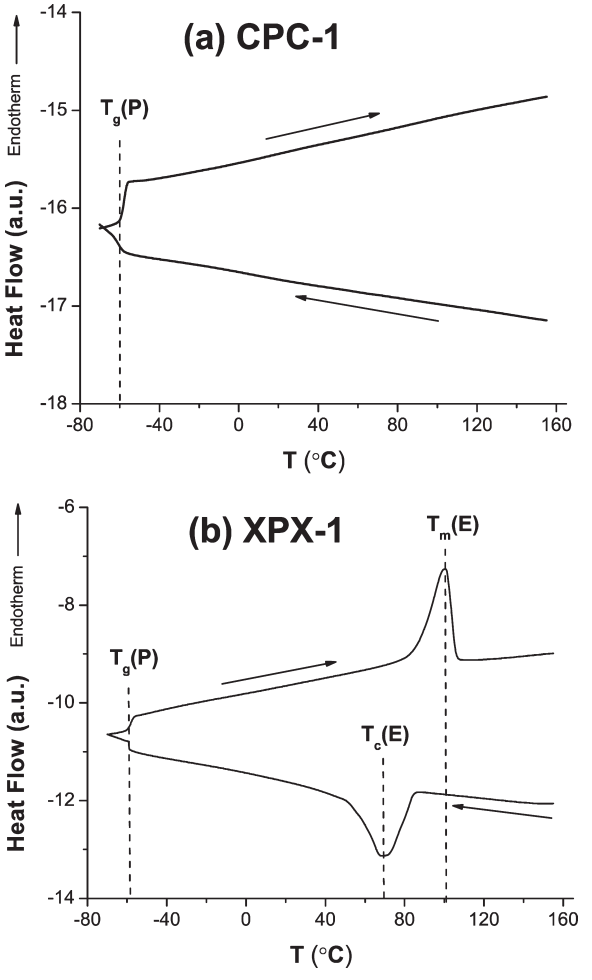

Figure 2. DSC traces obtained while heating and cooling (a) CPC-1 and (b) XPX-1 at 10 °C/min. T_g for P is evident in both specimens at about −60 °C. Melting and crystallization are apparent in XPX-1. However, the glass transition for C is not identified in either set of results.

Thermal and Rheological Properties. DSC measurements provided information regarding the physical properties of the CPC and XPX materials. Figure 2 offers a comparison of the responses obtained from representative specimens, each containing 18% C (see Table 1). Clearly evident in the thermal responses from CPC-1 (Figure 2a) and XPX-1 (Figure 2b) is a glass transition at −60 °C, which can be associated with the P domains.[27] We are not able to identify features in either DSC trace attributable to the glass transition of the C blocks; T_g of bulk C is about 145 °C. We believe this is a consequence of several factors. As shown below, XPX-1 is a homogeneous material above the E melting temperature, $T_{m,E}$; hence, there are no glassy domains above about 100 °C. While CPC-1 is microphase separated below 170 °C (see below), the combination of a minority of glassy domains (just 18%) and the proximity to T_{ODT} is most likely responsible for washing out any signature of T_g of C in the DSC trace from the material.

Table 2. Thermal Properties of CPC and XPX Copolymers

sample	T_m(E) (°C)[a]	T_c(E) (°C)[b]	X_c(E) (%)[c]	T_{ODT} (°C)[d]
CPC-1				168
CPC-2				172
XPX-1	100	68	36	$< T_m$
XPX-2a	98	56	32	$< T_m$
XPX-2b	97	54	26	$< T_m$
XPX-2c	93	55	22	$< T_m$
XPX-3	93	54	23	$< T_m$

[a] Peak melting temperature determined by DSC. [b] Peak crystallinity temperature determined by DSC. [c] Percent crystallinity in E block determined by DSC. [d] Order−disorder transition temperature detected by DMS.

The most prominent features in Figure 2b are the melting endotherm ($T_{m,E}$ = 100 °C) and crystallization exotherm ($T_{c,E}$ = 68 °C) found upon heating and cooling XPX-1, respectively. These thermal events, which derive from the partial local ordering of the poly(ethylene) blocks, play a pivotal role in driving the structural transitions that are responsible for the mechanical properties reported here. Table 2 summarizes the crystalline characteristics obtained by DSC for all the XPX heptablock copolymers considered in this article as well as the T_{ODT} values for the CPC materials. Consistent with previous work on block copolymers containing hydrogenated 1,4-poly(butadiene) with about 10% 1,2 additions, we obtain melting temperatures between 93 and 100 °C and 23%−36% crystallinity (X_c) of the E blocks based on the area under the peak in the melting curve.[4,8,28] Cooling at 10 °C/min results in peak rates of crystallization between 54 and 68 °C; this degree of hysteresis between $T_{m,E}$ and $T_{c,m}$ is attributable to polymer crystal nucleation.

Thermal transitions also were determined using dynamic mechanical spectroscopy (DMS). Representative dynamic elastic moduli, G', obtained from CPC-1 are displayed in Figure 3 as a function of reduced frequency ($a_T\omega$ where a_T is a temperature-dependent shift factor) at several temperatures and as a function of temperature at fixed frequency. The master curve obtained by time−temperature superposition of isothermal data (Figure 3a) exhibits two branches at low reduced frequencies consistent with states of order and disorder below and above about 170 °C, respectively.[24,29−34] This apparent T_{ODT} also is reflected in the isochronal temperature scan (Figure 3b) as a nearly discontinuous drop in G' at 168 °C. Evidence of a glass transition between approximately 100 and 140 °C is apparent in the $G'(T)$ curve as well. Similar DMS results were obtained from CPC-2, including a similar T_{ODT} at 172 °C (Table 2).

DMS was also performed on the XPX materials, and Figure 4 shows a representative master curve and a typical set of temperature sweep data obtained at 0.1 rad/s and 2 °C/min for XPX-1. Above 100 °C the $G'(\omega)$ results (Figure 4a) superpose onto a single master curve with a terminal slope, $G' \sim \omega^2$, consistent with liquid-like behavior.

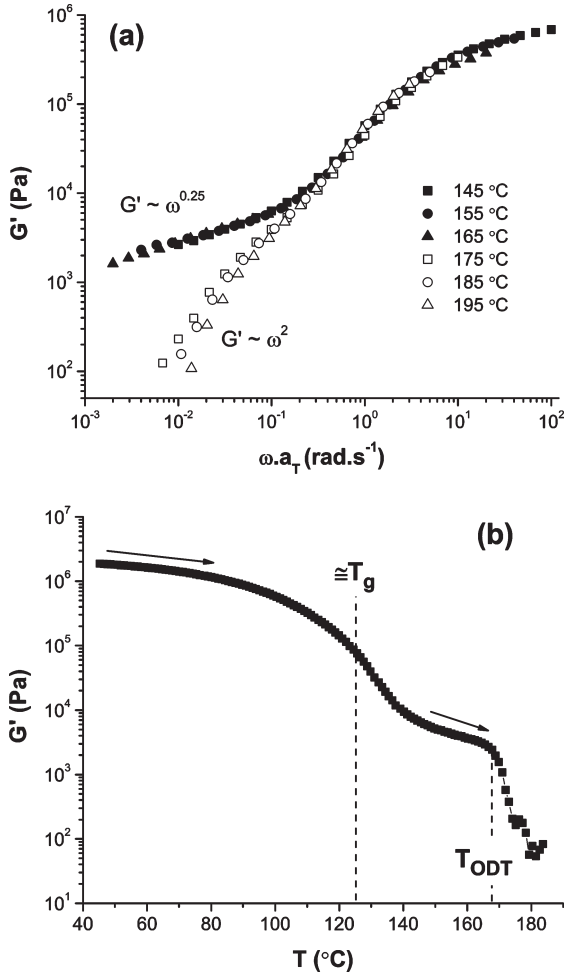

Figure 3. (a) Superposition of G' vs reduced frequency, ωa_T, from isothermal frequency sweeps with T_{REF} = 145 °C and (b) temperature sweep at 0.1 rad/s and 0.5 °C/min for CPC-1, both at 1% strain. A T_{ODT} of 168 °C produces a change of slopes in (a) and a discontinuity in (b) and T_g for C at around 125 °C is indicated by the decline in G' in (b).

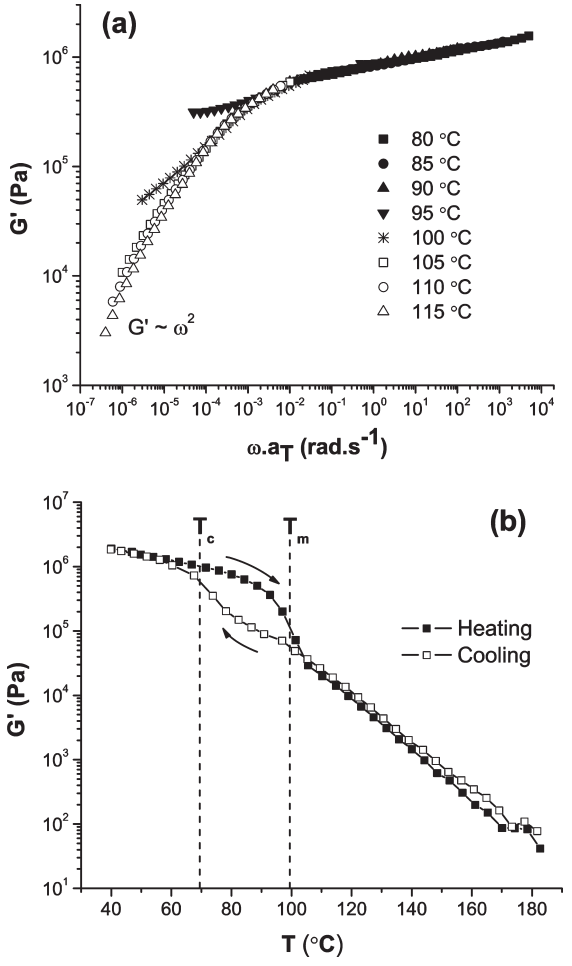

Figure 4. (a) Superposition of G' vs reduced frequency, ωa_T, from isothermal frequency sweeps with T_{REF} = 95 °C and (b) temperature sweep at 0.1 rad/s and 2 °C/min for XPX-1, both at 1% strain. Melting and crystallization dominate the thermal behavior of XPX.

Below 100 °C the low-frequency portions of the $G'(\omega)$ curves depart from the high-temperature master curve, indicative of a non-liquid-like response. Of course, we have already shown that XPX-1 is semicrystalline at and below about 100 °C based on DSC measurements (see Figure 2b). Heating and cooling XPX-1 leads to hysteresis in G' (Figure 4b) with end points that match the exotherm and endotherm identified in the DSC measurements (Figure 2b). Similar results were obtained from the other XPX heptablock copolymers, leading us to conclude that all these materials are liquid-like above $T_{m,E}$.

Structural Analysis. The morphologies of the CPC and XPX materials were investigated using small-angle X-ray scattering and transmission electron microscopy. The CPC triblocks were shear-aligned at about 160 °C using the procedures described by Koppi[25] and then interrogated by SAXS. Figure 5 shows a synchrotron SAXS pattern for CPC-1 at 25 °C and a laboratory source pattern for CPC-2 at 150 °C. CPC-1 and CPC-2 both produced SAXS patterns with multiple Bragg reflections at relative spacings $(q/q^*)^2$ = 1, 3, 4, and 7, where q^* is the position of the first-order reflection. These results are consistent with a hexagonally ordered arrangement of C cylinders embedded in a matrix of P polymer.[35−37] The magnitude of the principal wave vectors are related to the spacings between domains, $d^* = 2\pi/q^*$, where d^* corresponds to the separation between (11) planes

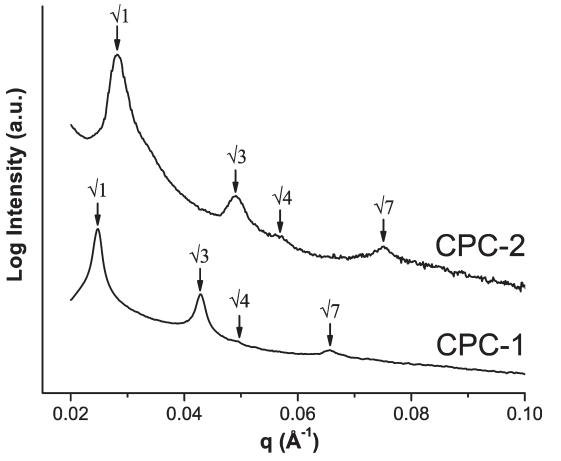

Figure 5. SAXS data acquired for shear-aligned samples of CPC-1 (synchrotron, 25 °C) and CPC-2 (laboratory, 150 °C) in the shear direction. Arrows indicate peak positions, which suggest a hexagonally packed cylindrical morphology for both materials below T_{ODT}. This structure is consistent with that expected for the block volume fractions.

in a hexagonally ordered crystal. These values are listed for CPC-1 and CPC-2 in Table 3.

Synchrotron SAXS data also were collected for the XPX systems at 140 and 25 °C, and the results are shown

Table 3. Domain Spacings Calculated from SAXS Data

sample	$q^*_{25\,°C}$ (Å^{-1})	$d^*_{25\,°C}$ (nm)	$q^*_{140\,°C}$ (Å^{-1})	$d^*_{140\,°C}$ (nm)
CPC-1	0.0249	25.2		
CPC-2			0.0284[a]	22.1[a]
XPX-3	0.0305	20.6	0.0286	22.0
XPX-2a	0.0299	21.0	0.0284	22.1
XPX-2b	0.0291	21.7	0.0270	23.3
XPX-2c	0.0276	22.8	0.0268	23.4
XPX-1	0.0205	30.6	0.0199	31.6

[a] Measured at 150 °C.

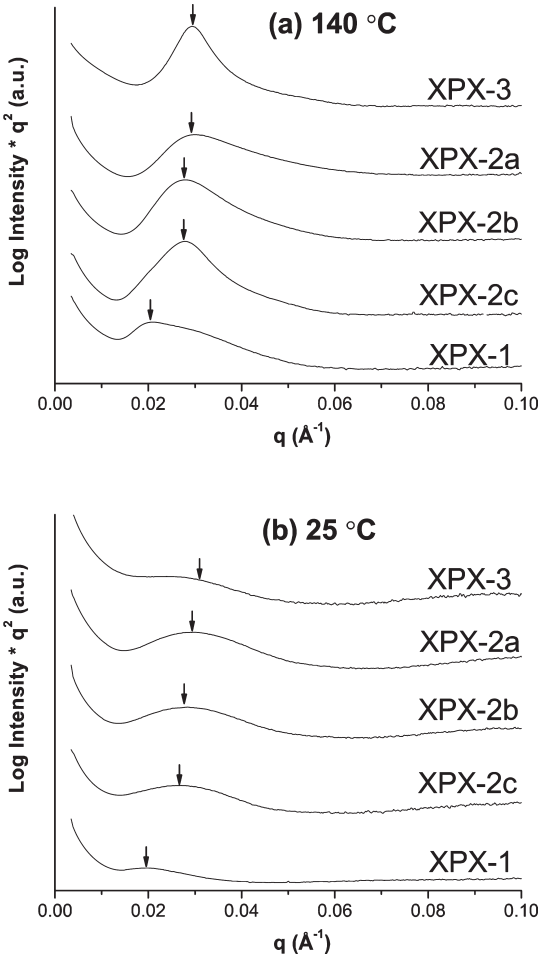

Figure 6. Synchrotron SAXS data acquired at (a) 140 °C and (b) 25 °C for XPX block copolymers. They each produce one relatively broad peak at both temperatures, which indicates the materials do not contain long-range order.

in Figure 6. In striking contrast to the SAXS patterns obtained from the CPC materials, every XPX heptablock displays only one rather broad peak at both temperatures, indicating that long-range order is absent in these materials. Curiously, the single broad peak is more intense at the higher temperature (consistent with earlier results),[14,28] which we assume reflects some degree of contrast matching in the microphase-separated state at 25 °C. Since DMS measurements have established that the XPX polymers are liquid-like above about 100 °C, we associate the peak in $I(q)$ at 140 °C with correlation hole scattering. Remarkably, q^* varies only slightly between the three XPX-2 compounds (see Table 3) despite the fact that these polymers have the same composition profile but differ in molecular weight by nearly a factor of 2. Moreover, q^*, and thus d^*, change very little from 140 to 25 °C for each material: d^* values drop only about 0.9 nm on average with cooling. We return to these features in the Discussion section.

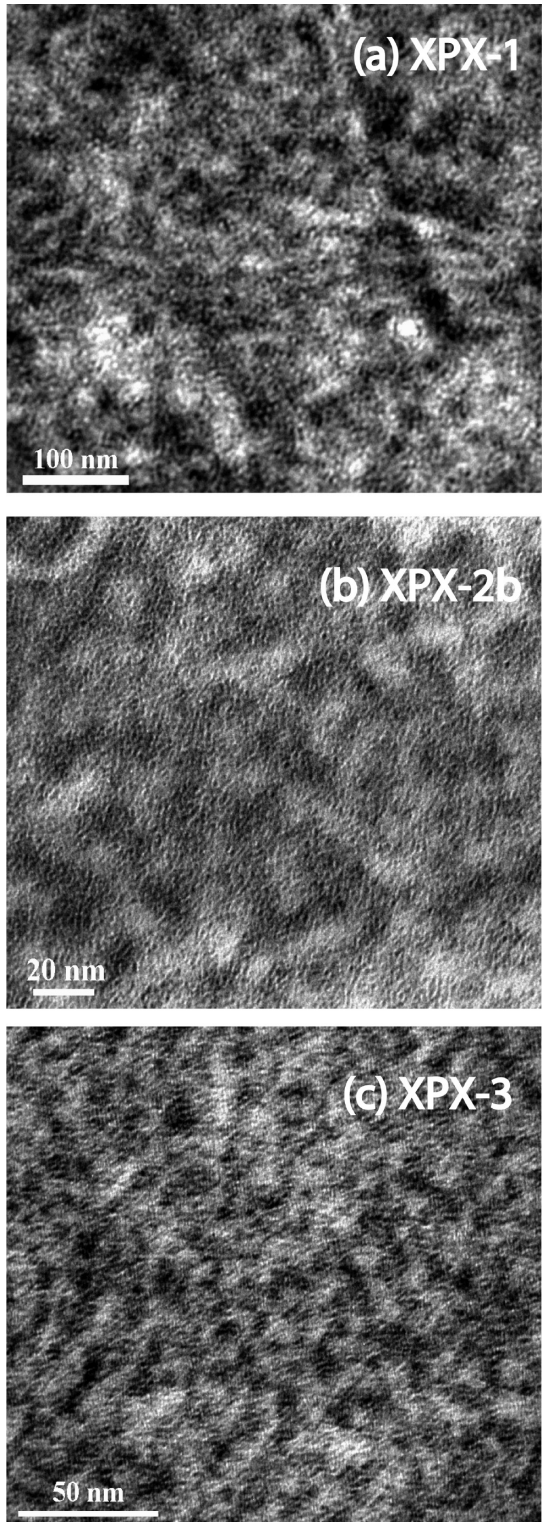

Figure 7. TEM images from (a) XPX-1, (b) XPX-2b and (c) XPX-3. All XPX materials show a disorganized morphology of C (gray), E (white), and P (black) domains.

TEM images were obtained from the XPX polymers to further delineate the microphase-separated structures present at room temperature. Representative TEM images recorded from XPX-1, XPX-2b, and XPX-3 are presented in Figure 7. Staining with RuO_4 creates contrast among the monomers resulting in images with black (P), gray (C), and

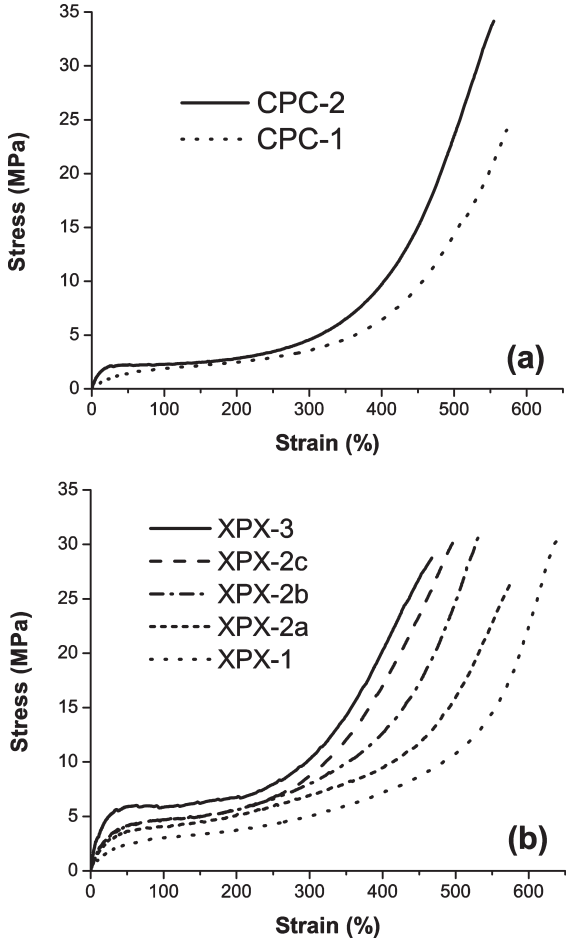

Figure 8. Representative engineering stress vs strain curves for (a) CPC copolymers and (b) XPX copolymers. XPX materials behave as strong thermoplastic elastomers with tensile strengths comparable to the strong CPC-2.

white (E) regions. All XPX images show rather disorganized structures with evidence of light and dark regions on a length scale that is compatible with the SAXS results (see Table 3). A combination of poor contrast, a lack of order, and ill-defined domain structure makes it impossible to assign a specific shape or packing geometry to these structural features. Nevertheless, the TEM images indicate some form of microphase separation and confirm the state of disorder deduced from the SAXS data.

Tensile Properties. Rectangular samples were subjected to uniaxial tensile testing at a rate of 200% strain/min at room temperature. Figure 8 compares representative tensile data taken from each material evaluated in this study. Table 4 summarizes five measures of mechanical behavior for these materials, elastic modulus E, strain at break ε_b, tensile strength (stress at break) σ_{TS}, final residual strain ε_r, and tension set ε_s (see Strain Recovery section) extracted from each set of eight measurements or three in the case of ε_r performed on each material. Here we note that our use of rectangular specimens, which almost always failed near the grips of the instrument, leads to conservative estimates of ε_b and σ_{TS}.

The CPC materials (Figure 8a) behave as typical thermoplastic triblock copolymer elastomers, combining high elongation with a low modulus and relatively high strength values. CPC-2 exhibits a higher modulus and tensile strength than CPC-1, which is attributable to a higher glass content.[1,2] Glassy domains act as cross-linkers and stiff filler particles, which can result in greater reinforcement (i.e., higher modulus and strength).

Table 4. Tensile Properties of CPC and XPX Block Copolymers

sample	E (MPa)	ε_b (%)	σ_{TS} (MPa)	ε_r (%)	ε_s (%)
CPC-1	5.5 ± 0.8	543 ± 33	22.2 ± 5.3	30 ± 5	11 ± 7
CPC-2	20.6 ± 5.0	552 ± 5	32.8 ± 2.2	44 ± 4	16 ± 6
XPX-1	10.0 ± 1.9	652 ± 23	26.9 ± 4.5	57 ± 3	31 ± 14
XPX-2a	19.2 ± 4.5	616 ± 32	25.8 ± 4.1	178 ± 3	84 ± 23
XPX-2b	21.9 ± 1.9	551 ± 11	30.5 ± 3.1	120 ± 11	64 ± 4
XPX-2c	24.0 ± 3.2	528 ± 19	32.1 ± 5.8	114 ± 3	80 ± 19
XPX-3	41.8 ± 6.3	509 ± 40	29.6 ± 2.8	198 ± 3	97 ± 20

All the XPX heptablock copolymers behave like strong thermoplastic elastomers (Figure 8b). In fact, all the XPX materials are statistically as strong as CPC-2, with tensile strengths between 26 and 32 MPa. Several interesting features emerge in comparing the XPX and CPC systems. The modulus (E) and stress plateau during drawing (strains up to about 200%) are higher for XPX than CPC at comparable glass contents due to the presence of the semicrystalline E blocks; this effect resembles a previous comparison of melt-ordered CPEPC and CPC.[14] Both C and E content have an important effect on the magnitude of the modulus. With 67% higher C content the modulus E for CPC-2 is nearly 4 times that for CPC-1. Similarly, adding semicrystalline E to XPX also stiffens the material. Comparing XPX-1 to CPC-1 and XPX-3 to CPC-2, each pair having similar amounts of C, indicates that the semicrystalline blocks double the moduli. However, this reinforcement of XPX at low strains does not translate into a higher strength. In general, tensile strengths in both CPC and XPX samples seem to have a maximum value of about 32 MPa. Nor do we find any statistical difference between XPX and CPC with respect to strain at break, which are about 550% for all materials, except for XPX-1 and XPX-2a, which extend to slightly higher elongation of 652% and 612%, respectively. However, this may stem from molecular weight differences, which are evident in the XPX-2 series. While all three XPX-2 materials have statistically similar moduli and tensile strengths, XPX-2a has a strain at break of 616%, modestly different than the average 540% for the two higher molecular weight systems. XPX heptablocks with lower molecular weight seem to produce "softer" materials that fail at significantly higher elongation.

Strain Recovery. Cyclic testing (strain and recovery) was performed on samples by stretching them to 400% strain (about 70% of their average strain at break) and then compressing the specimen to 0% strain and repeating this sequence for a total of seven cycles. Residual strain was identified after each cycle as the deformation (strain) at which the measured stress disappeared (σ = 0 MPa) as the sample length was reduced back toward its original value.

Residual strain is plotted as a function of cycle number in Figure 9 for all the materials considered in this report. These measurements are remarkably reproducible as evidenced by the narrow range of values shown, about 5% variation. The final residual strains after seven cycles, ε_r, are shown for each material in Table 4. Tension set values, ε_s, also presented in Table 4, are approximately half of ε_r for each material and show a similar trend of increasing irrecoverable deformations. However, these results have high uncertainty levels given the difficulty in manually measuring the final length of rubbery samples, and thus our analysis is focused on the results of cyclic testing. All samples tend to reach a constant residual strain, especially the XPX compounds; after four cycles these materials add less than 5% additional residual strain on average by the seventh cycle. The CPC copolymers

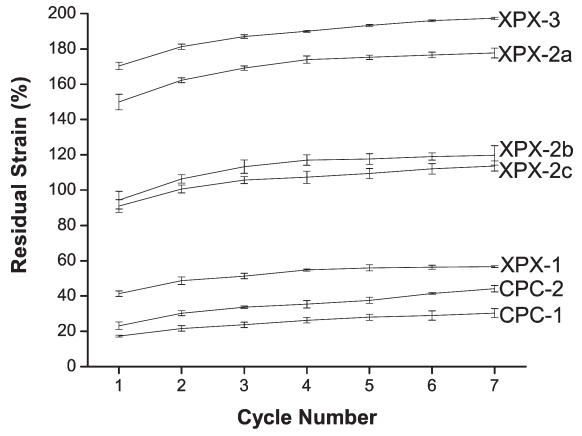

Figure 9. Residual strain after cyclic deformation up to 400% strain for CPC and XPX materials. Higher C and E content increases residual strain while an increase in molecular weight in the XPX-2 series improves recoverability.

show the least residual strains, which is readily explained by the hard glassy C domains, which offer little if any irreversible deformation.[13,14,18,37,38] Increasing the C content from 18% (CPC-1) to 30% (CPC-2) marginally lifts ε_r from 30% to just 44%.

Incorporation of semicrystalline E blocks in the XPX materials has a significant impact on the elastic recovery of these specimens. Prior work with semicrystalline TPEs has led to the conclusion that plastic crystal deformation is responsible for nonrecoverable strain.[4,10,12−14,18,19] Increasing the E content raises the amount of residual strain in the XPX compounds from 54% to 120% to 197% for 22% E (XPX-1) to 26% E (XPX-2b) to 28% E (XPX-3), respectively. However, the C content also increases equally, and the effects of the added crystallinity and glass cannot be decoupled. Most importantly, the ill-defined morphology of the XPX elastomers may reorganize irreversibly during large strain extension, which could contribute to a larger residual strain, particularly as the C and E content increases. Figure 9 also shows the residual strain curves for the XPX-2 series, which have a constant composition but varying molecular weights. Here strain recovery increases as the overall molecular weight decreases. XPX-2a (M_n = 79 000 g/mol) exhibits a 178% residual strain after seven cycles while XPX-2c (M_n = 114 000 g/mol) recovers all but 114%. Thus, XPX materials seem to require a minimum molecular weight to achieve optimal mechanical properties.

Discussion

Phase Behavior and Morphology. A combination of rheological measurements, SAXS, and TEM revealed different types of phase behavior and different morphologies for the CPC versus the XPX systems. The CPC triblock copolymers produce classical, here hexagonally ordered, phases that pass through a first-order transition to a disordered melt state at a temperature (T_{ODT}) that is determined by the overall polymer molecular weight (and composition). Microphase separation at low temperatures is driven by thermodynamic incompatibility between the C and P blocks, which is captured by the magnitude of the Flory−Huggins segment−segment interaction parameter, $\chi_{CP} = (V/RT)(\delta_C - \delta_P)^2$, where V is the segment volume and δ_C and δ_P are the solubility parameters of the C and P polymers, respectively. Notwithstanding close chemical similarities, most pairs of saturated hydrocarbon polymers such as C and P, C and E, and E and P are characterized by small but positive χ parameters. In fact, C and P have been shown to have nearly the same segment−segment interaction parameter as the unsaturated precursor polymers S and I, i.e., $\chi_{CP} \approx \chi_{SI}$.[33] This explains why CPC triblock copolymers order at modest molecular weights and CPC-1 and CPC-2 have $T_{ODT} \cong 170$ °C. Extensive investigations of numerous hydrogenated diblock copolymers have led to the following relative classifications: $\delta_C < \delta_P < \delta_E$ leading to $\chi_{EP} \ll \chi_{CP} < \chi_{CE}$.[39] These thermodynamic factors have been exploited in designing the XPX heptablock copolymers.

The molecular design of the XPX heptablocks creates terpolymers that are melt disordered, even at relatively high overall molecular weights. The molecular weights of the C and E blocks in the X portions of the molecules have been chosen to permit these polymers to mix above the melting point of the E blocks ($T_m \sim 100$ °C). A nearly symmetric (42% C) CEC triblock with M_n = 30 kg/mol has a T_{ODT} of about 220 °C.[14] Therefore, the CEC portions of the XPX molecules were kept below this critical value. XPX-2c has the largest X sequences, 28.5 kg/mol, which might be expected to induce segregation between the E and C blocks at a temperature above 100 °C. However, a second factor favors mixing of the C, E, and P blocks above T_m. In the homogeneous state P segments can make contact with E and C segments, and both these interactions are favored over C−E contacts. Alternatively, the mixed CEC portions of the heptablock copolymer present an average solubility parameter $(\delta_C\delta_E)^{1/2}$ that is close to δ_P, which promotes overall homogeneity.

Crystallization disrupts this delicate balance. C blocks will be ejected from the vicinity of the crystallizing E blocks, which then cascades into segregation of P. We do not have a detailed understanding of either the dynamics of this process or the resulting structure. However, there is strong evidence to support our conclusion that the low-temperature morphology contains largely separate E, C, and P domains. DSC traces from XPX-1 (Figure 2b) evidence a sharp glass transition at about −60 °C, which is clearly associated with nearly pure poly(ethylene-*alt*-propylene). These thermal measurements also reveal poly(ethylene) melting temperatures and extents of crystallization (Table 2) that are typical of E-based diblock, triblock, and multiblock copolymers.[4,8,9,28] There is little direct evidence for the presence of separate C domains, although discrete E and P material makes this an inescapable conclusion. We were not able to identify a glass transition temperature for poly(cyclohexylethylene) in any of the polymers examined by DSC, including the CPCs, for reasons discussed earlier. DMS experiments are complicated by crystallization and melting (Figure 4b) over the same range of temperatures where we expect to see the effects of vitrification. Unfortunately, the morphologies revealed in the TEM images are too disorganized to permit the reliable assignment of specific domain structures.

Above 100 °C mixing of C, E, and P leads to a homogeneous viscoelastic fluid with a hypothetical glass transition temperature that is well below 100 °C, i.e., between that of pure C (ca. 140 °C) and amorphous E and P (< -50 °C). A liquid-like low-frequency rheological response (Figure 4) supports this notion. Segregation of C blocks from E blocks during nucleation and growth of poly(ethylene) crystals is accompanied by vitrification of the former, thereby arresting the development of equilibrium domain structures with long-ranged order. The net effects of these highly nonequilibrium processes are irregularly shaped microdomains with ill-defined internal placement of C and E, which are randomly distributed within the material. While crystallization triggers microphase separation we believe that the glassy portion of

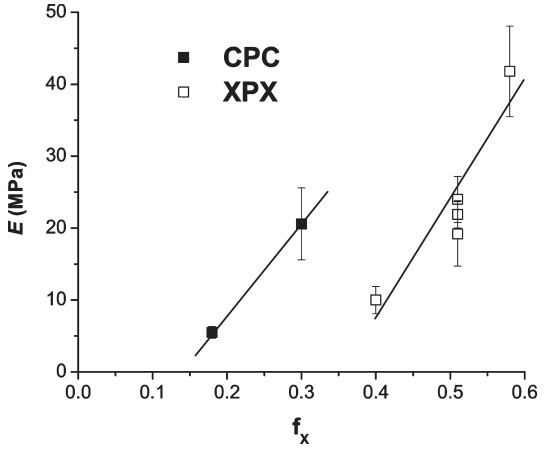

Figure 10. Elastic moduli of CPC and XPX materials vs $f_X = f_C + f_E$ shows that C cylinders stiffen the materials more than the X blocks.

the resulting microdomains anchors the P blocks to the particles, rendering high strength. Indeed, previous work with EPE triblock copolymers has shown that crystallization-induced ordering from the disordered melt state results in rather weak elastomers.[4,8]

The scale of this structural development is controlled by the overall dimensions of the heptablock copolymer as shown by the SAXS measurements obtained at 140 and 25 °C (Figure 6 and Table 3). Broad and low-intensity SAXS peaks above T_m can be attributed to correlation hole scattering, which derives from a ~15% melt density difference between poly(cyclohexylethylene) and poly(propylene); the melt densities of E and P are equal. Crystals of E will nucleate with dimensions significantly smaller than the overall molecular size, and the submolecular scale distribution of E and C domains will be immobilized by the vitrification of the microphase-separated C before long-range order can be established. Thus, the morphology reflects the same average spacing as the correlation hole in the disordered melt.

On the basis of purely Gaussian statistics, the random phase approximation anticipates $d^* \sim N^{1/2}$ at constant composition. Despite composition differences, the values of $d^* = 2\pi/q^*$ for XPX-1 and XPX-3 follow this scaling. On the other hand, values for the XPX-2 polymers do not scale correctly with the rest of the data, especially as we increase M_n. Specifically, the peak position q^* for XPX-2a should appear at 1.39 times higher value than q^* for XPX-2c; clearly this is not the case. While we do not understand the exact origins of this experimental result, we should note that increasing N changes the segregation strength and may activate inhomogeneous composition fluctuations in the disordered melt (i.e., between C and E vs C and P vs E and P blocks), which are not accounted for in the simple scaling prediction. (Also puzzling is that disordered CECEC−P hexablocks exhibit two correlation hole peaks[19] while disordered CEC−P−CEC and CECEC−P−CECEC[19] multiblocks produce only one.) This issue will be taken up in a future publication.

Tensile Properties. Tensile tests (Figure 8) show that all the block copolymers investigated in this study exhibit thermoplastic elastic behavior with certain similarities and differences. Any similarity is rather surprising given the dramatic difference in morphology between the CPC and XPX materials. While we have not been able to establish a detailed structure for the XPX compounds, TEM results suggest a random arrangement of X and P domains with an ill-defined state of connectivity. This contrasts sharply with the classical highly ordered cylindrical domain structure found with the CPC polymers (Figure 5).

In the small strain limit the linear elastic modulus E is correlated to the hard content or $f_X = f_C + f_E$ for both CPC and XPX, as illustrated in Figure 10. The X blocks are less effective at stiffening the material than the C cylinders. Most likely this is a morphological effect (hexagonally ordered cylinders vs disordered and possibly disconnected particles), or it may reflect the composite nature of the X microdomains, i.e., softer semicrystalline E combined with glassy C. It takes roughly twice the volume fraction of X relative to C to obtain the same modulus in XPX as CPC. These data also suggest that the XPX materials are all continuous in rubbery P and most likely are not continuous in X. Prior reports have documented that the room temperature linear elastic modulus of nearly symmetric isotropic CEC triblock copolymers with $f_C \sim 0.42-0.61$ is $E \sim 156-410$ MPa.[14,40] A bicontinuous arrangement of this material with an equal volume fraction of rubbery P polymer would be expected to yield a modulus of roughly 80−200 MPa, an order of magnitude greater that what we measure. Therefore, we conclude that the XPX compounds contain largely disconnected hard particles composed of segregated semicrystalline E and glassy C.

All the block copolymers investigated in this study displayed similar tensile properties at large deformation with strain to break values falling between 500 and 650% and tensile strengths ranging from 22 to 33 MPa (Table 4). Similarity in ε_b and σ_{TS} between CPC and XPX indicates that the ultimate properties are governed primarily by the rubbery P matrix. We can conclude from these findings that the X particles in XPX are as effective at anchoring the P molecules as the C domains in CPC. Poly(ethylene-*alt*-propylene) (P) is a densely entangled polymer with a molecular weight between entanglements M_e = 1475 g/mol at room temperature.[22] All the polymers under consideration in this work are highly entangled, containing more than 10 entanglements per center P block. The ultimate strength of an entangled rubber is controlled by the number of entanglements per rubbery chain and the strength of the anchors that restrain the chain ends. Although we are not aware of a quantitative theoretical treatment of this problem, the insensitivity of the measured tensile strengths to reinforcing particle type (C vs X) offers strong evidence that the limits of particle mechanical integrity have not been realized. This finding represents a significant accomplishment of our investigation. In summary, X nanoparticles containing C and E domains generated through crystallization-induced microphase separation provide at least as much mechanical reinforcement to thermoplastic elastomers as conventional glassy microdomains.

Strain Recovery. In contrast to the single extension large strain properties discussed in the previous paragraph, there are significant differences in the strain recovery characteristics between CPC and XPX. Irreversible deformation in rubbery thermoplastic elastomers generally is correlated with the content and morphological connectivity of hard domains.[37,41−43] As with the modulus analysis (Figure 10), the residual strain after seven cycles, as well as the tension set, are different for CPC vs XPX as a function of f_X ($= f_C + f_E$), as shown in Figure 11. Apparently changing f_X has a much more dramatic effect on the permanent deformation of the XPX elastomers than on the CPC materials. However, it is not possible to separate the effects of the brittle glassy C and plastic semicrystalline E components on strain recovery in XPX. Also, while we have documented a common hexagonal morphology for CPC-1 and CPC-2, we have not established

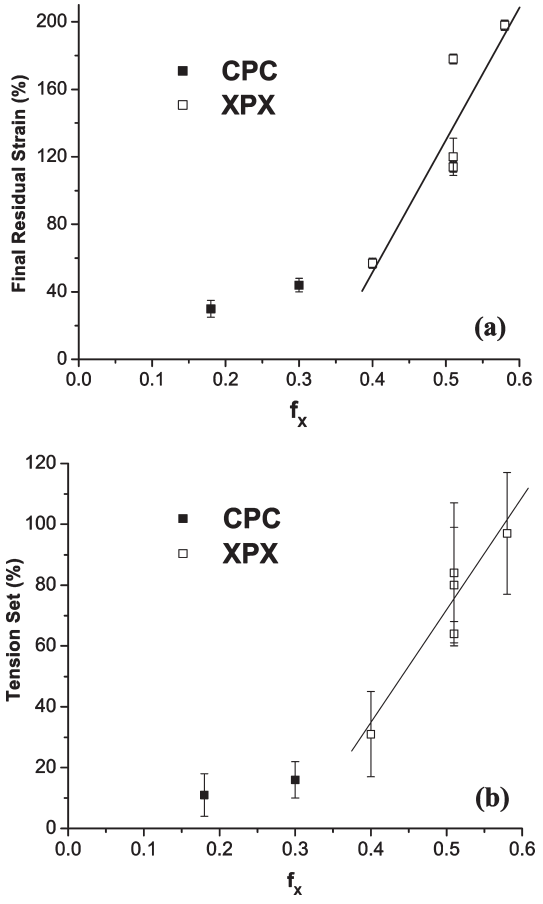

Figure 11. (a) Final residual strain after seven cycles of deformation to 400% strain, and (b) tension set, vs $f_X = f_C + f_E$ for both CPC and XPX materials. XPX materials with residual strains comparable to CPC (about 44%) can be achieved when $f_X \leq 0.39$.

how increasing f_X in the XPX materials influences the morphology, particularly the connectivity of the X domains, with the potential for irreversible distortion and breakup during extension.

An important implication of Figure 11a is that the residual strain in XPX materials will approach or exceed the performance of CPC when $f_X \leq 0.39$ even at a somewhat greater hard block content. This may be a consequence of morphological differences, i.e., glassy C cylinders vs isolated X domains. We expect most morphological changes to occur in a given material during the first 400% deformation cycle, which is supported by the result found in Figure 9. All the experimental curves in Figure 9 share a common form with the largest contribution to permanent set occurring in the first cycle followed by a more modest evolution of nonrecoverable strain during subsequent extension and recovery cycles. Clearly, the strain remaining after the first deformation cycle as well as the tension set values (Figure 11b) parallel the final residual strain plotted as a function of f_X in Figure 11a.

Thus, CPC and XPX experience maximum disruption of hard domains in the first extension where morphology and in particular its state of connectivity influence the type of deformation. Then, the random and more discrete (as evidenced by the values of modulus) arrangement of hard X particles in XPX may be able to produce materials as recoverable as CPC despite a higher composition of hard domains. Thus, generating XPX copolymers with $f_X \leq 0.39$ should yield materials as strong and recoverable as CPC but with the advantage of disordering at a fixed temperature given by $T_{m,E}$, independent of molecular weight up to a limiting value, which allows for low-temperature processing.

Finally, the XPX-2 series of polymers revealed that varying the molecular weight has important effects on tensile and recovery properties, which has significant implications regarding the mechanisms of deformation in these materials. The two higher molecular weight XPX-2 materials, XPX-2b and XPX-2c with $M_n = 79$ and 114 kg/mol, respectively, had similar values of ultimate tensile strength, strain at break, and residual strain. On the other hand, the lowest molecular weight material, XPX-2a with $M_n = 59$ kg/mol, was statistically just as strong but failed at a higher extension and experienced a significantly higher residual strain. That the ultimate strength remains constant provides further evidence that in XPX the strength limit of the hard particles is not reached and failure likely occurs due to rubber rupture.

Conclusion

A new class of thermoplastic multiblock copolymer elastomers with a CEC−P−CEC heptablock molecular architecture, denoted XPX, was prepared and characterized for structure and tensile properties. XPX materials contained between 42% and 60% poly(ethylene-*alt*-propylene) (P), and all CEC block sequences combined equal fractions of poly(cyclohexylethylene) (C) and poly(ethylene) (E). CPC triblock elastomers with 18% and 30% C also were analyzed for comparison. Thermal analysis by DSC and DMS showed that the CPC compounds microphase separate in the melt with T_{ODT} at about 170 °C. The molecular configuration of the XPX terpolymers results in disordered materials above the melting temperature, $T_{m,E}$, of the E blocks for all specimens up to 114 000 g/mol in molecular weight. Thermal, SAXS, and TEM measurements indicate that the XPX materials microphase separate upon crystallization of the E blocks, resulting in a disordered arrangement of particles containing C and E domains dispersed in a rubbery P matrix. Both CPC specimens form conventional hexagonally packed (glassy) cylinders below T_{ODT}. Single extension and cyclic tensile tests were performed on all materials to assess and compare the mechanical properties of XPX and CPC. All the XPX materials were statistically as strong as the CPC elastomers with ultimate tensile strengths ranging from 26 to 32 MPa and strains at break between 500% and 650%. This indicates that microphase-separated X particles, comprised of equal amounts of semicrystalline E and glassy C, are as reinforcing as C cylinders in CPC, notwithstanding crystallization-induced segregation. Also, a uniform ultimate strength suggests that the limit of strength of these hard X particles has not been reached and that the rupture of the rubber middle block dictates material failure. Residual strain, following seven cycles of tensile deformation to 400% strain, was found to be dependent on both composition and molecular weight. A relatively low elastic modulus for all XPX samples, 10−42 MPa, suggests a disconnected morphology of X regions, which may account for the substantial elastic recovery. On the basis of the extrapolation of this property, we anticipate that XPX elastomers will exhibit equal or better recovery than the CPC compounds when the fraction of X domains, $f_X = f_C + f_E \leq 0.39$. Thus, CEC−P−CEC heptablock terpolymers provide strong and recoverable elastomeric materials with the advantage of possessing a common processing temperature dictated by $T_{m,E}$ which is decoupled from molecular weight below a critical value.

Acknowledgment. The authors express gratitude to the Medtronic Corporation and the National Science Foundation (DMR-0704192) for financial and logistical support of this project. The Characterization Facility of the Institute of Technology

at the University of Minnesota receives partial support from the National Science Foundation through the NNIN program and the Materials Research Science and Engineering Center (NSF-MRSEC) at the University of Minnesota (NSF DMR-0212302). SAXS was performed at the DuPont−Northwestern−Dow Collaborative Access Team (DND-CAT) located at sector 5 of the Advanced Photon Source (APS) at Argonne National Laboratory. DND-CAT is supported by E. I. du Pont de Nemours & Co., The Dow Chemical Company, and the State of Illinois. Use of the APS was supported by the U.S. Department of Energy, Office of Science, Office of Basic Energy Sciences, under Contract DE-AC02-06CH11357.

Supporting Information Available: A figure of ^{1}H NMR characterization of XPX-3 and its unsaturated precursor, SBS−I−SBS-3. This material is available free of charge via the Internet at http://pubs.acs.org.

References and Notes

(1) Holden, G.; Bishop, E. T.; Legge, N. R. *J. Polym. Sci., Part C* **1969**, 37−57.
(2) Holden, G.; Legge, N. R.; Quirk, P. R.; Schroeder, H. E. *Thermoplastic Elastomers*, 2nd ed.; Hanser Publishers: New York, 1996.
(3) Fredrickson, G. H.; Bates, F. S. *Annu. Rev. Mater. Sci.* **1996**, *26*, 501–550.
(4) Seguela, R.; Prudhomme, J. *Polymer* **1989**, *30* (8), 1446–1455.
(5) Cohen, R. E.; Cheng, P. L.; Douzinas, K.; Kofinas, P.; Berney, C. V. *Macromolecules* **1990**, *23* (1), 324–327.
(6) Rangarajan, P.; Register, R. A.; Fetters, L. J. *Macromolecules* **1993**, *26* (17), 4640–4645.
(7) Nandan, B.; Hsu, J. Y.; Chen, H. L. *Polym. Rev.* **2006**, *46* (2), 143–172.
(8) Koo, C. M.; Wu, L. F.; Lim, L. S.; Mahanthappa, M. K.; Hillmyer, M. A.; Bates, F. S. *Macromolecules* **2005**, *38* (14), 6090–6098.
(9) Koo, C. M.; Hillmyer, M. A.; Bates, F. S. *Macromolecules* **2006**, *39* (2), 667–677.
(10) Hotta, A.; Cochran, E.; Ruokolainen, J.; Khanna, V.; Fredrickson, G. H.; Kramer, E. J.; Shin, Y. W.; Shimizu, F.; Cherian, A. E.; Hustad, P. D.; Rose, J. M.; Coates, G. W. *Proc. Natl. Acad. Sci. U. S.A.* **2006**, *103* (42), 15327–15332.
(11) Wang, H. P.; Khariwala, D. U.; Cheung, W.; Chum, S. P.; Hiltner, A.; Baer, E. *Macromolecules* **2007**, *40* (8), 2852–2862.
(12) Mohajer, Y.; Wilkes, G. L.; Wang, I. C.; McGrath, J. E. *Polymer* **1982**, *23* (10), 1523–1535.
(13) Schmalz, H.; Boker, A.; Lange, R.; Krausch, G.; Abetz, V. *Macromolecules* **2001**, *34* (25), 8720–8729.
(14) Mahanthappa, M. K.; Lim, L. S.; Hillmyer, M. A.; Bates, F. S. *Macromolecules* **2007**, *40* (5), 1585–1593.
(15) Mahanthappa, M. K.; Hillmyer, M. A.; Bates, F. S. *Macromolecules* **2008**, *41* (4), 1341–1351.
(16) Balsamo, V.; Gil, G.; de Navarro, C. U.; Hamley, I. W.; von Gyldenfeldt, F.; Abetz, V.; Canizales, E. *Macromolecules* **2003**, *36* (12), 4515–4525.
(17) Balsamo, V.; de Navarro, C. U.; Gil, G. *Macromolecules* **2003**, *36* (12), 4507–4514.
(18) Schmalz, H.; Abetz, V.; Lange, R. *Compos. Sci. Technol.* **2003**, *63* (8), 1179–1186.
(19) Fleury, G.; Bates, F. S. *Macromolecules* **2009**, *42* (10), 3598–3610.
(20) Ndoni, S.; Papadakis, C. M.; Bates, F. S.; Almdal, K. *Rev. Sci. Instrum.* **1995**, *66* (2), 1090–1095.
(21) Hucul, D. A.; Hahn, S. F. *Adv. Mater.* **2000**, *12* (23), 1855–1858.
(22) Fetters, L. J.; Lohse, D. J.; Richter, D.; Witten, T. A.; Zirkel, A. *Macromolecules* **1994**, *27* (17), 4639–4647.
(23) Brandrup, J.; Immergut, E. H. *Polymer Handbook*, 3rd ed.; John Wiley & Sons: New York, 1989.
(24) Rosedale, J.; Bates, F. S.; Almdal, K.; Mortensen, K.; Wignall, G. D. *Macromolecules* **1995**, *28* (5), 1429–1443.
(25) Koppi, K. A. Ph.D. Thesis, Department of Chemical Engineering, University of Minnesota, Minneapolis, MN, 1993.
(26) Khandpur, A. K.; Macosko, C. W.; Bates, F. S. *J. Polym. Sci., Part B: Polym. Phys.* **1995**, *33* (2), 247–252.
(27) Gotro, J. T.; Graessley, W. W. *Macromolecules* **1984**, *17* (12), 2767–2775.
(28) Weimann, P. A.; Hajduk, D. A.; Chu, C.; Chaffin, K. A.; Brodil, J. C.; Bates, F. S. *J. Polym. Sci., Part B: Polym. Phys.* **1999**, *37* (16), 2053–2068.
(29) Bates, F. S.; Rosedale, J. H.; Fredrickson, G. H.; Glinka, C. J. *Phys. Rev. Lett.* **1988**, *61* (19), 2229–2232.
(30) Bates, F. S.; Rosedale, J. H.; Fredrickson, G. H. *J. Chem. Phys.* **1990**, *92* (10), 6255–6270.
(31) Rosedale, J. H.; Bates, F. S. *Macromolecules* **1990**, *23* (8), 2329–2338.
(32) Gehlsen, M. D.; Almdal, K.; Bates, F. S. *Macromolecules* **1992**, *25* (2), 939–943.
(33) Gehlsen, M. D.; Bates, F. S. *Macromolecules* **1993**, *26* (16), 4122–4127.
(34) Kossuth, M. B.; Morse, D. C.; Bates, F. S. *J. Rheol.* **1999**, *43* (1), 167–196.
(35) Seguela, R.; Prudhomme, J. *Macromolecules* **1978**, *11* (5), 1007–1016.
(36) Bates, F. S.; Fredrickson, G. H. *Annu. Rev. Phys. Chem.* **1990**, *41*, 525–557.
(37) Honeker, C. C.; Thomas, E. L.; Albalak, R. J.; Hajduk, D. A.; Gruner, S. M.; Capel, M. C. *Macromolecules* **2000**, *33* (25), 9395–9406.
(38) Patel, R. M.; Hahn, S. F.; Esneault, C.; Bensason, S. *Adv. Mater.* **2000**, *12* (23), 1813–1817.
(39) Cochran, E. W.; Bates, F. S. *Macromolecules* **2002**, *35* (19), 7368–7374.
(40) Hermel, T. J. Ph.D. Thesis, Department of Chemical Engineering, University of Minnesota, Minneapolis, MN, 1993; p 71.
(41) Odell, J. A.; Keller, A. *Polym. Eng. Sci.* **1977**, *17* (8), 544–559.
(42) Pakula, T.; Saijo, K.; Kawai, H.; Hashimoto, T. *Macromolecules* **1985**, *18* (6), 1294–1302.
(43) Honeker, C. C.; Thomas, E. L. *Chem. Mater.* **1996**, *8* (8), 1702–1714.